Molecular Therapy
Nucleic Acids
Original Article

# Decoding CKD-induced muscle atrophy through the critical role of lncRNA GAS5 and pyroptosis

Rong Huang,[1,2] Xinying Tang,[1,2] Shuang Liu,[1,2] and Lijing Sun[1]

[1]Department of Nephrology, Xinhua Hospital Affiliated to Shanghai Jiaotong University School of Medicine, Shanghai 200092, China

**Skeletal muscle atrophy is a prevalent complication of chronic kidney disease (CKD) and serves as an indicator of adverse prognosis and poor quality of life; however, the underlying mechanisms remain ambiguous. Emerging evidence has shown that long non-coding RNAs (lncRNAs) are involved in the pathogenesis of skeletal muscle atrophy. Using RNA sequencing (RNA-seq), we discerned elevated GAS5 expression in the muscles of CKD mice and verified these findings by real-time qPCR. Transmission electron microscopy confirmed morphological signs of pyroptosis, a potentially causal cellular death form. Additionally, elevated levels of pyroptosis markers, such as NLRP3, cleaved caspase-1, and GSDMD-N, were observed in CKD mouse models and lipopolysaccharide (LPS)/ATP-stimulated C2C12 myotubes. Intriguingly, the knockdown of GAS5 reduced these markers, alleviating pyroptosis and enhancing myofiber size, both *in vitro* and *in vivo*. Furthermore, we pinpointed an interaction between GAS5 and the mitochondrial translation elongation factor (TUFM) through RNA pull-down and mass spectrometry. This interaction amplified NLRP3 activity, contributing to pyroptosis and muscle atrophy. Notably, overexpressing TUFM counterbalanced this effect. Fundamentally, the interaction between GAS5 and TUFM appears to compromise the anti-pyroptosis capacity of TUFM. Consequently, this amplifies the activation of the NLRP3 pathway, which may underpin the crucial mechanism driving pyroptosis-mediated muscle atrophy. Our findings provide new evidence for GAS5's role in regulating cellular pyroptosis in CKD-induced skeletal muscle atrophy.**

## INTRODUCTION

Chronic kidney disease (CKD) poses a significant public health challenge that affects >10% of the general population worldwide, amounting to >800 million individuals. CKD has emerged as one of the leading causes of death globally, with its mortality rate increasing over the past few decades. Importantly, CKD represents a large medical burden in many countries.[1] Skeletal muscle atrophy is a common complication of CKD, characterized by a decline in skeletal muscle mass and diminished muscle functionality.[2] As an independent risk factor for mortality, skeletal muscle atrophy is closely associated with the quality of life and adverse prognosis in patients with CKD. However, the mechanisms leading to muscle atrophy in patients with CKD remain unclear, and treatment options are very limited.

Various molecular mechanisms contribute to the development of muscle atrophy. Evidence suggests that cell death may play a pivotal role in inducing muscle atrophy.[3,4] Pyroptosis, a novel form of programmed cell death that follows apoptosis and necrosis, is characterized by the production of oligomeric N-terminal fragments by the protein GSDMD. This process leads to the formation of pores on the host cell membrane (CM), resulting in cell lysis and death.[5] The most typical pyroptosis activation pathway is mediated by nucleotide-binding oligomerization domain (NOD)-like receptors (NLRs).[6] The successive activation of NLRP3 and caspase-1 facilitates the cleavage of gasdermin D, releasing inflammatory cytokines interleukin (IL)-1β and IL-18.[7–9] It has been reported that NLRP3-mediated pyroptosis can lead to dexamethasone-induced skeletal muscle atrophy, and knocking down NLRP3 can alleviate this response.[10] Similarly, in AngII-induced skeletal muscle atrophy, the knockout of NLRP3 also demonstrated a protective effect against muscle atrophy.[11] Recent studies have indicated that pyroptosis plays a key role in diabetic-induced skeletal muscle atrophy and muscle weakness.[12] An increasing number of reports indicate that pyroptosis is involved in the mechanism of muscle atrophy. Still, few studies comprehensively reveal the role of pyroptosis in CKD-induced skeletal muscle atrophy.

Long non-coding RNAs (lncRNAs) are a class of nucleotide RNAs that do not encode proteins and have a transcription length exceeding 200 nt.[13] Studies have shown that lncRNAs play vital regulatory roles in various biological processes, such as apoptosis, metabolism, and the cell cycle.[14] An increasing body of evidence also indicates that lncRNAs exert crucial functions in various disease processes, such as inflammatory diseases, cancer, and cardiovascular diseases, by regulating pyroptosis.[15–17] Accumulating evidence supports that

Received 3 August 2024; accepted 10 January 2025;
https://doi.org/10.1016/j.omtn.2025.102451.

[2]These authors contributed equally

**Correspondence:** Lijing Sun, Department of Nephrology, Xinhua Hospital Affiliated to Shanghai Jiaotong University School of Medicine, Shanghai 200092, China.
**E-mail:** sunlijing@xinhuamed.com.cn

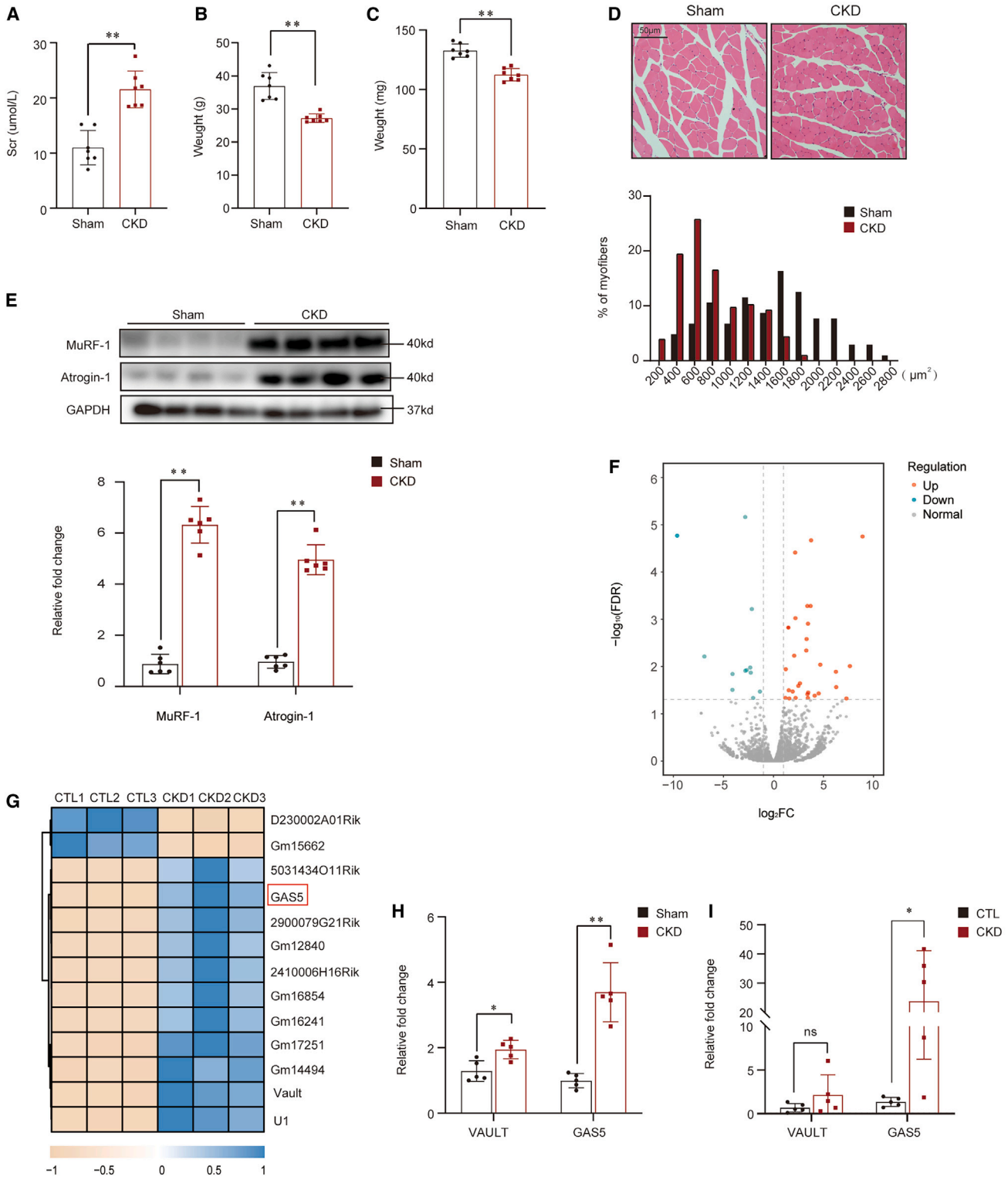


**Figure 1. Identification of differentially expressed lncRNAs in skeletal muscle atrophy of CKD mice**

(A) Serum creatinine levels in sham mice and CKD mice ($n$ = 6, $^{**}p < 0.01$). (B) Comparison of body weights between sham mice and CKD mice ($n$ = 6, $^{**}p < 0.01$). (C) Comparison of gastrocnemius muscle weights between sham mice and CKD mice ($n$ = 6, $^{**}p < 0.01$). (D) H&E staining shows a reduction in muscle cross-sectional area

*(legend continued on next page)*

lncRNAs may play direct or indirect roles upstream of the pyroptosis trigger pathway.[18] Recent research showed that lncRNA TINCR could promote pyroptosis by positively regulating NLRP3 in diabetic cardiomyopathy, while METTL14 suppresses pyroptosis and diabetic cardiomyopathy by downregulating TINCR lncRNA.[19] The aberrant expression of lncRNAs is associated with the pathogenesis of muscle atrophy. Our previous research demonstrated that lncRNA Atrolnc-1 is involved in the occurrence of muscle atrophy in CKD.[20] However, the underlying mechanism of lncRNAs regulating the pyroptosis pathway in muscle atrophy with CKD is not clear.

In this study, we identified a novel CKD-associated lncRNA and clarified its function in muscle atrophy. The lncRNA GAS5 exhibited a markedly elevated expression in the CKD muscle atrophy model. We also found that after GAS5 interacts with TUFM, it enhances NLRP3 activity, activates the pyroptosis pathway, and leads to the occurrence of pyroptosis. These findings provide new evidence for GAS5's role in regulating cellular pyroptosis in CKD-induced skeletal muscle atrophy and offer new insights for the prevention and treatment of muscle atrophy.

## RESULTS

### Identification of differentially expressed lncRNAs in skeletal muscle atrophy of CKD mice

To probe the potential role of lncRNAs in CKD-associated skeletal muscle atrophy, we utilized RNA sequencing (RNA-seq) analysis on quadriceps femoris muscles from control and CKD mice. We induced CKD in 12-week-old *C57BL6* mice via a 5/6 nephrectomy procedure. Four weeks post-operation, when compared with sham-operated controls, CKD mice manifested elevated serum creatinine levels (Figure 1A) and a significant decrease in both body and individual gastrocnemius muscle weights (Figures 1B and 1C). Histological evaluation using hematoxylin and eosin (H&E) staining highlighted a pronounced reduction in the muscle cross-sectional area (CSA) in CKD mice compared to the results of controls (Figure 1D, top). Further analysis of the CSA showcased a left-shifted muscle fiber distribution in the CKD group (Figure 1D, bottom). Corresponding with these protein energy wasting (PEW) phenotypic changes, we observed elevated expressions of the atrophy-associated genes MuRF-1 and Atrogin-1 in the quadriceps femoris muscles of CKD mice, as evidenced by 6- and 5-fold increases, respectively, in the western blot analysis (Figure 1E). After post-validation of muscle atrophy phenotypes in CKD mice, we delved into the lncRNA profiles within their muscles. The volcano plot provided an overview of all differentially expressed lncRNAs (Figure 1F). Using criteria that required at least two counts per million (CPM) >0 in each group and a false discovery rate (FDR) < 0.01, we identified 13 lncRNAs differentially expressed in CKD mice muscles. Of these, 11 were upregulated, and 2 were downregulated, as illustrated in the heatmap (Figure 1G). Prioritizing lncRNAs of potential clinical significance to humans, we focused on homologous molecules between human and mouse lncRNA pools (Figure S1). This led to the exclusion of 11 non-human-specific lncRNAs. Among the remaining two lncRNAs, GAS5 emerged as the most significantly upregulated lncRNA shared between humans and mice, pinpointing it as our primary molecule of interest. To substantiate our RNA-seq findings, we validated GAS5 expression levels using real-time qPCR in skeletal muscle tissues from both the CKD mouse models and patients with end-stage renal disease (ESRD). This confirmed the pronounced elevation of GAS5 expression in both groups (Figures 1H and 1I). Collectively, our results underscore the elevated expression of GAS5 in the atrophic skeletal muscles of CKD mice. This suggests a potential regulatory interplay between GAS5 expression and CKD-induced muscle atrophy.

### Unraveling the protein interactome of GAS5 in CKD muscle

After observing elevated levels of GAS5 in the muscles of CKD mice, we aimed to uncover its potential role in muscle atrophy. We first assessed the cellular distribution of GAS5 by fluorescence *in situ* hybridization (FISH) on C2C12 cells and mouse muscle tissues. Using a FAM-labeled Gas5 probe, we found that GAS5 is primarily localized in the cytoplasm, although a small fraction is also present in the nucleus. This dual localization suggests that GAS5 may have roles in both signaling and gene regulation (Figure 2A). Given that lncRNAs are known to influence signaling pathways by interacting with specific proteins,[21,22] we hypothesized that GAS5 might function through its association with certain proteins. To explore this, we performed RNA pull-down experiments using C2C12 myotube extracts (Figure 2B), followed by mass spectrometry (MS) to identify proteins interacting with the biotin-labeled GAS5 probe. Our analysis revealed that GAS5 is associated with over 45 proteins (Figure 2C; Table S1). Subsequent pathway enrichment analysis using KEGG highlighted a significant involvement of GAS5-associated proteins in the NLR signaling pathway, which is essential for inflammasome formation and chronic inflammatory responses (Figure 2D). Among the proteins, TUFM caught our attention due to its known role in inhibiting NLRP3 inflammasome formation.[23] To confirm this interaction, we used immunoblotting with an anti-TUFM antibody. A distinct protein band, corresponding to the expected molecular weight of TUFM, was found among the proteins associated with biotinylated GAS5 (Figure 2E). Furthermore, RNA immunoprecipitation (RIP) experiments were performed with an antibody against TUFM or negative immunoglobulin (Ig)G, and immunoprecipitation using anti-TUFM antibodies from C2C12 myotube lysates followed by real-time qPCR showed significant enrichment of GAS5, whereas control (IgG) precipitates displayed undetectable levels of GAS5

(CSA) in CKD mice (top). Scale bar: 50 μm. The distribution of myofiber sizes in CKD mice was shifted leftward (bottom). (E) Western blot confirmed the expression levels of MuRF-1 and Atrogin-1 in muscles of CKD mice ($n = 6$, $^{**}p < 0.01$). (F) The volcano plots display all differentially expressed lncRNAs. (G) Heatmap shows the top 13 differentially expressed lncRNAs in quadriceps muscles of CKD mice and sham mice. (H) Real-time qPCR confirmed the upregulation of GAS5 and VAULT in CKD mice ($n = 5$, $^{*}p < 0.05$ and $^{**}p < 0.01$). (I) Real-time qPCR confirmed the upregulation of GAS5 and VAULT in muscles of patients with ESRD ($n = 5$, ns: no statistically significant difference, $^{*}p < 0.05$).

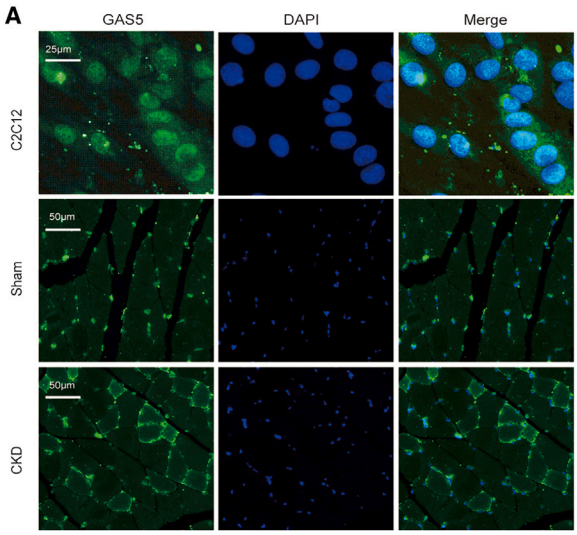


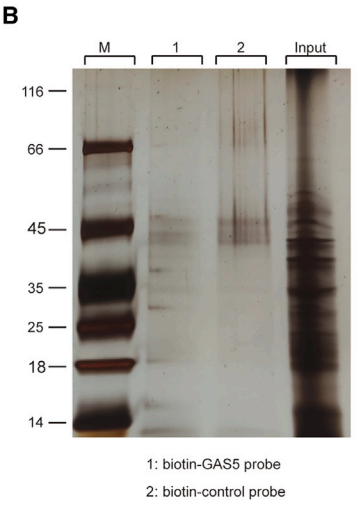


C

| Protein | iBAQ Control | iBAQ GAS5 |
|---|---|---|
| Rab6b | 0.00 | 48.59 |
| Iqcf3 | 0.00 | 43.87 |
| Tecr | 0.00 | 26.33 |
| Rpl3 | 0.00 | 16.61 |
| Mfsd10 | 0.00 | 15.06 |
| Sdhc | 0.00 | 11.97 |
| TUFM | 0.00 | 7.51 |
| Arpc2 | 0.00 | 5.89 |
| Capza2 | 0.00 | 3.02 |
| Phb | 0.00 | 1.73 |

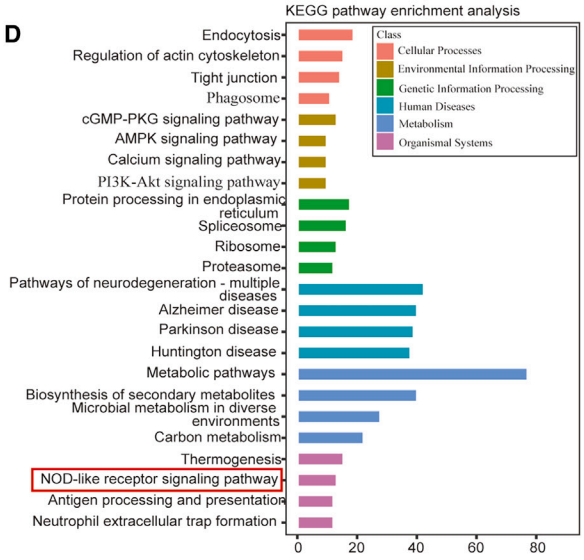


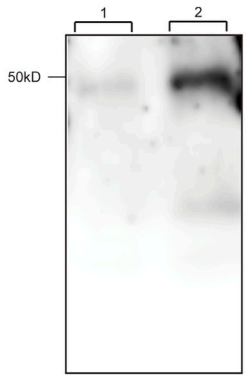


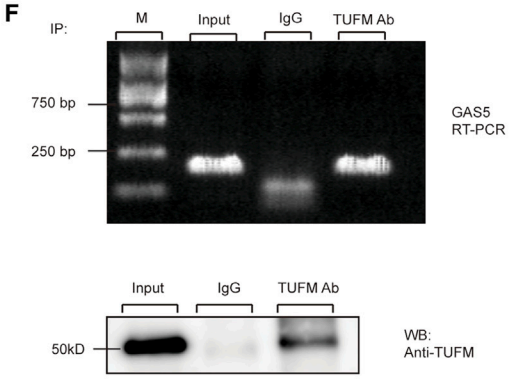


*(legend on next page)*

(Figure 2F). Collectively, these results demonstrated a direct interaction between GAS5 and TUFM and point to a potential role for GAS5 in regulating NLRP3-associated pathways, particularly in the context of CKD-induced muscle atrophy.

### Linking GAS5 upregulation with pyroptosis and atrophic responses in C2C12 myotubes

Given that activation of NLRP3-associated pathways frequently culminates in pyroptosis across various cell types, we aimed to devise an *in vitro* model of pyroptosis using C2C12 myotubes. The lipopolysaccharide (LPS)/ATP stimulation method is widely used in research to induce an inflammatory response, activate immune signaling pathways, and trigger relevant intracellular mechanisms, particularly through activation of the NLRP3 pathway to further enhance inflammation. Utilizing a well-documented approach, we treated C2C12 myotubes with LPS (100 ng/mL; Sigma) for 2 h, followed by ATP (5.0 mM; Med Chem Express) for another 1 h to induce intracellular inflammatory responses.[10] Subsequent analysis via western blotting revealed a marked elevation in the expression of pyroptosis-related proteins. Specifically, levels of NLRP3, cleaved caspase-1, GSDMD, GSDMD-N, and IL-1β showed significant increases, with GSDMD expression being the most prominent (Figure 3A). To further corroborate the occurrence of pyroptosis, we employed Hoechst 33342/PI double staining, which confirmed significant pyroptotic activity in the LPS/ATP-stimulated C2C12 myotubes (Figure 3B). Importantly, this LPS/ATP stimulation also led to a robust upregulation of GAS5 expression (Figure 3C). Additionally, to assess the potential link between NLRP3 pathway activation and myotube atrophy, we observed a notable reduction in the diameter of C2C12 myotubes following LPS/ATP stimulation (Figure 3D). Concurrently, there was a pronounced increase in the expression of muscle-atrophy-associated proteins, MuRF-1 and Atrogin-1 (Figure 3E). In summation, our established *in vitro* model effectively linked NLRP3 pathway activation to myotube atrophy. Furthermore, this model offers a valuable platform to further investigate the role of GAS5 in regulating both pyroptosis and myotube atrophy processes.

### Knockdown of GAS5 improves LPS/ATP-induced pyroptosis and atrophy in C2C12 myotubes

To investigate the regulatory role of GAS5 in myotube atrophy and pyroptosis, we employed an adeno-associated virus 1 (AAV1) vector bearing shGAS5 to knock down GAS5 in C2C12 myotubes. We first ensured the transfection efficiency by using an AAV1 vector with GFP (AAV1-GFP) and observed that nearly 100% of the myofibers expressed GFP (Figure S2). Following this, we transfected C2C12 myotubes with either control AAV1 (AAV1-CTL) or AAV1-shGAS5 for 48 h. Subsequent treatment with LPS/ATP for 3 h was employed to induce pyroptosis. Using real-time qPCR, we observed that LPS/ATP-induced upregulation of GAS5 was significantly inhibited in the AAV1-shGAS5 transfected myotubes, with GAS5 levels decreasing by approximately 90% compared to the AAV1-CTL-transfected myotubes (Figure 4A). Further investigation using immunoblot analysis revealed that the LPS/ATP-induced expression of both atrophy-related proteins (MuRF-1 and Atrogin-1) and pyroptosis-associated proteins, including NLRP3, cleaved caspase-1, GSDMD, GSDMD-N, and the inflammatory cytokine IL-1β, was markedly suppressed upon GAS5 knockdown (Figure 4B). We further found that LPS/ATP-induced reduction in the diameter of C2C12 myotubes was partially improved by GAS5 knockdown (Figure 4C). In addition, Hoechst 33342/PI double staining highlighted a significant reduction in LPS/ATP-induced pyroptosis in the GAS5-knockdown C2C12 cells compared to the controls (Figure 4D). In conclusion, our findings demonstrate that GAS5 knockdown effectively ameliorates both cellular pyroptosis and myotube atrophy induced by LPS/ATP in C2C12 myotubes.

### TUFM overexpression counteracts GAS5-driven NLRP3 activation and pyroptosis in C2C12 myotubes

To understand the intricate role of TUFM in regulating NLRP3 activity, we employed an AAV1 to overexpress the TUFM gene (AAV1-TUFM). Given existing literature highlighting TUFM's inhibitory effects on NLRP3-mediated pyroptosis and our observations of GAS5's interaction with TUFM, we hypothesized that GAS5 might negate this inhibition. Following transfection of C2C12 myotubes with AAV1-TUFM, we noted an 11-fold surge in TUFM mRNA levels (Figure 5A). Immunoblot analysis revealed that the expression of TUFM was markedly increased upon TUFM overexpression, indicating effective transfection (Figure 5B). This process resulted in diminished pyroptosis-related protein levels in the AAV1-TUFM transfected myotubes; concurrently, MuRF-1 and Atrogin-1 expression levels also showed a decline (Figure 5C). Complicating the narrative, our data revealed diminished TUFM levels in both CKD mice and LPS/ATP-stimulated C2C12 myotubes when compared to their respective controls (Figure 5D). Concomitant with these results, an LPS/ATP-induced reduction in the diameter of C2C12 myotubes could be improved by TUFM overexpression (Figure 5E). The interaction between GAS5 and TUFM may present dual outcomes. On one hand, GAS5 seems to counteract the inhibitory effect of TUFM. On the other hand, GAS5 might compromise the stability of TUFM. In aggregate, these impacts underscore the central role of the GAS5-TUFM interaction in catalyzing the NLRP3-mediated pyroptosis pathway. Overall, our findings shed light on the intricate interplay between GAS5 and TUFM, elucidating their potential roles in modulating NLRP3-mediated pyroptosis, a possible factor in CKD-induced muscle atrophy.

**Figure 2. Unraveling the protein interactome of GAS5 in CKD muscle**

(A) Fluorescence *in situ* hybridization(FISH) analysis of C2C12 cells and muscles from mice. GAS5-positive signal manifests as green fluorescence. (B) SDS-PAGE displays the results of RNA pull-down assay. (C) Mass spectrometry (MS) identified proteins that specifically interact with GAS5. (D) KEGG pathway enrichment analysis indicated signaling pathways linked to GAS5 expression. (E) A representative immunoblotting shows a band at 50 kD using TUFM antibody in the proteins pulled down by biotin-labeled GAS5 probe. (F) Real-time PCR was used to quantify GAS5 in immunoprecipitates (top). Western blot shows a band at 50 kD in the immunoprecipitation (IP) product using TUFM antibody (bottom).

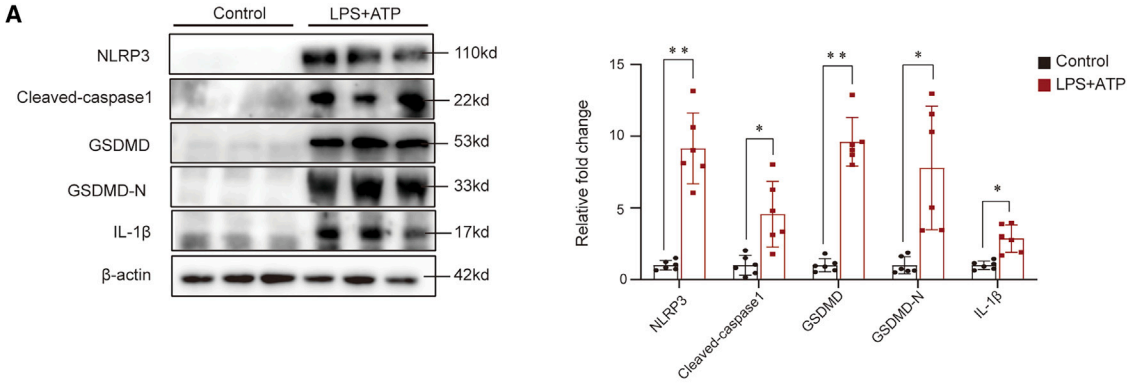


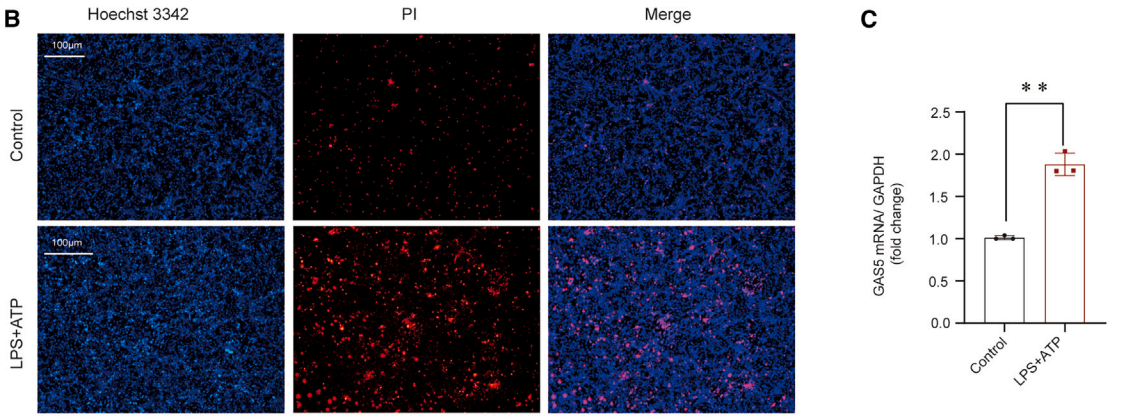


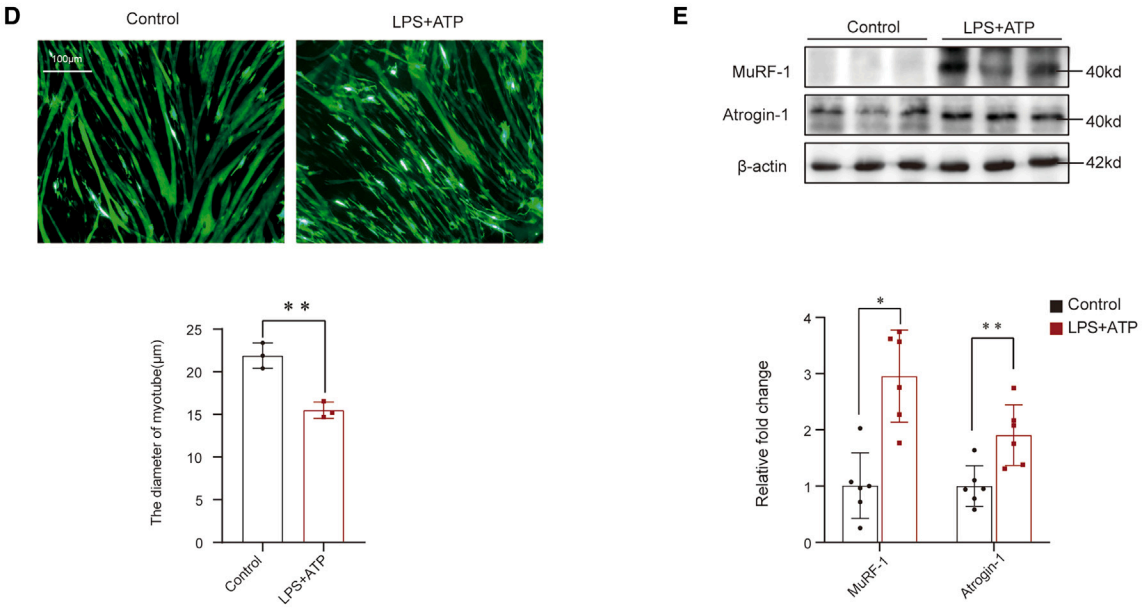


*(legend on next page)*

### Evidence linking pyroptosis to muscle atrophy in CKD mice

Previous studies have implicated inflammation, particularly pyroptosis, in the progression of muscle atrophy.[24] To investigate the presence of pyroptosis in skeletal muscles of CKD mice, we employed transmission electron microscopy (TEM). Our observations revealed marked alterations in the skeletal muscles of CKD mice compared to the sham control group. Specifically, we noted increased occurrences of membrane rupture and mitochondrial damage; large sections of the skeletal muscle CM displaying discontinuities, forming extensive holes (highlighted with red arrows in Figure 6A); swelling and enlargement of organelles, partial rupture of muscle fibers (denoted by yellow arrows in Figure 6A), and areas of muscle fiber fusion and thickening; symmetrically distributed sarcomeres, with the majority of myofibrillar filaments exhibiting dense structures and minor areas displaying ruptures; and mitochondria (M) interspersed among muscle fibers, characterized by significant swelling, matrix dissolution, and vacuolation (Figure 6A, left). We found that the nuclei (N) in muscle cells are irregularly shaped and that the nuclear membrane remains intact in the CKD group; we also noticed the condensation of chromatin (Figure 6A, blue arrows), while in the sham control group, the nuclear chromatin is evenly distributed (Figure 6A, right). These morphological features are characteristic of pyroptosis. To corroborate our morphological findings, we probed for molecular markers of pyroptosis in CKD mouse muscles. Western blot analysis demonstrated elevated expression levels of pyroptosis-associated proteins, including NLRP3, cleaved caspase-1, GSDMD, GSDMD-N, and IL-1β, in CKD mice when compared to sham controls (Figure 6B). Similarly, immunofluorescence (IF) staining underscored heightened expression of NLRP3 and cleaved caspase-1 in CKD mouse skeletal muscles (Figure 6C). Taken together, our results provide both morphological and molecular evidence for the occurrence of pyroptosis in the skeletal muscle atrophy instigated by CKD.

### Knockdown of GAS5 alleviates cellular pyroptosis and muscle atrophy in CKD mice

Given the observed regulatory effect of GAS5 on LPS/ATP-induced pyroptosis and skeletal muscle atrophy in C2C12 myotubes, we hypothesized that GAS5 might play a similar role in an *in vivo* context. We injected either AAV1-shGAS5 or AAV1-CTL into the quadriceps of sham control and CKD mice via intramuscular injection (Figure S3). As illustrated in Figure 7A, GAS5 mRNA levels in CKD mice injected with AAV1-shGAS5 were significantly lower than those in CKD mice injected with AAV1-CTL, indicating a successful GAS5 knockout in the CKD model. Immunoblot analysis revealed that in comparison to the CKD+AAV1-CTL group, the CKD+AAV1-shGAS5 group exhibited significantly reduced expression of MuRF-1, Atrogin-1, and pyroptosis-related proteins such as NLRP3, cleaved caspase-1, GSDMD, GSDMD-N, and IL-1β (Figure 7B). These findings were further corroborated by IF staining of muscles from CKD mice, which consistently displayed reduced expression levels of NLRP3 and cleaved caspase-1 (Figure 7C). Notably, the muscle CSA in the CKD+AAV1-shGAS5 group showed significant improvement compared to the CKD+AAV1-CTL group, suggesting that GAS5 knockout can attenuate the loss of skeletal muscle mass in CKD mice (Figure 7D). This assertion was further supported by the shift in the distribution of muscle fiber CSA observed after GAS5 knockout (Figure 7E). In summary, our results demonstrate that GAS5 knockout can mitigate both cellular pyroptosis and muscle atrophy in CKD mice.

## DISCUSSION

This study discovered that GAS5 regulates skeletal muscle atrophy in CKD through the activation of the NLRP3 signaling pathway. First, we observed a marked increase in the expression of GAS5 in atrophied skeletal muscles in CKD. GAS5 interacts with the pyroptosis inhibitory factor TUFM, mediated by the NLRP3 signaling pathway. This interaction reduces the inhibitory effect of TUFM on NLRP3, leading to an enhanced activity of the NLRP3 signaling pathway, resulting in increased pyroptosis and skeletal muscle atrophy (Figure 8). Apart from demonstrating that GAS5 is one of the molecules involved in regulating muscle atrophy, we also proved that knocking out GAS5 can alleviate pyroptosis and muscle atrophy, while overexpressing TUFM can inhibit pyroptosis and improve skeletal muscle atrophy.

Pyroptosis mediated by NLRP3 is an essential mechanism for the occurrence of muscle atrophy.[25] Several studies in non-CKD-induced muscle atrophy models have confirmed this notion. For instance, Yan et al. reported that treating ischemia-induced skeletal muscle cell pyroptosis with exosomes containing circHIPK3 can reduce NLRP3 activation and caspase-1 cleavage and improve mouse muscle strength.[26] Similarly, in dexamethasone-induced muscle atrophy, extracts from the leaves of *Ageratum conyzoides* could inhibit muscle degradation by blocking the nuclear factor κB (NF-κB)/NLRP3-mediated pyroptosis pathway.[27] Further studies indicated that the upregulation of glycolysis in the muscle tissues of patients with idiopathic inflammatory myopathies activated NLRP3, causing muscle cell pyroptosis and leading to muscle weakness.[28] It has been reported that IL-1β, an activation product of the pyroptosis pathway, can act directly on muscle cells, resulting in skeletal muscle atrophy. By knocking out NLRP3, the activation of IL-1β can be inhibited, thus preventing muscle atrophy in critically ill patients.[29] As we know, the inflammatory signaling pathway is an important cause of organ damage.[30] Our study further confirmed that, in skeletal muscle

**Figure 3. Linking GAS5 upregulation with pyroptosis and atrophic responses in C2C12 myotubes**

(A) The protein levels of NLRP3, cleaved caspase-1, GSDMD, GSDMD-N, and IL-1β were detected in C2C12 myotubes by western blot ($n = 6$, $^{*}p < 0.05$ and $^{**}p < 0.01$). (B) Detection of pyroptotic activity in the LPS/ATP-stimulated C2C12 myotubes by dual staining with Hoechst 33342 and PI. (C) Real-time qPCR result shows increased GAS5 mRNA level in the LPS/ATP-stimulated C2C12 myotubes ($n = 3$, $^{**}p < 0.01$). (D) Fluorescence images display notable reduction in the diameter of C2C12 myotubes following LPS/ATP stimulation (top). Scale bar: 100 μm. Graphic presentation of myotube diameter in different groups (bottom). (E) Western blot analysis confirmed the upregulation of MuRF-1 and Atrogin-1 expression levels in the LPS/ATP-stimulated C2C12 myotubes ($n = 6$, $^{*}p < 0.05$ and $^{**}p < 0.01$).

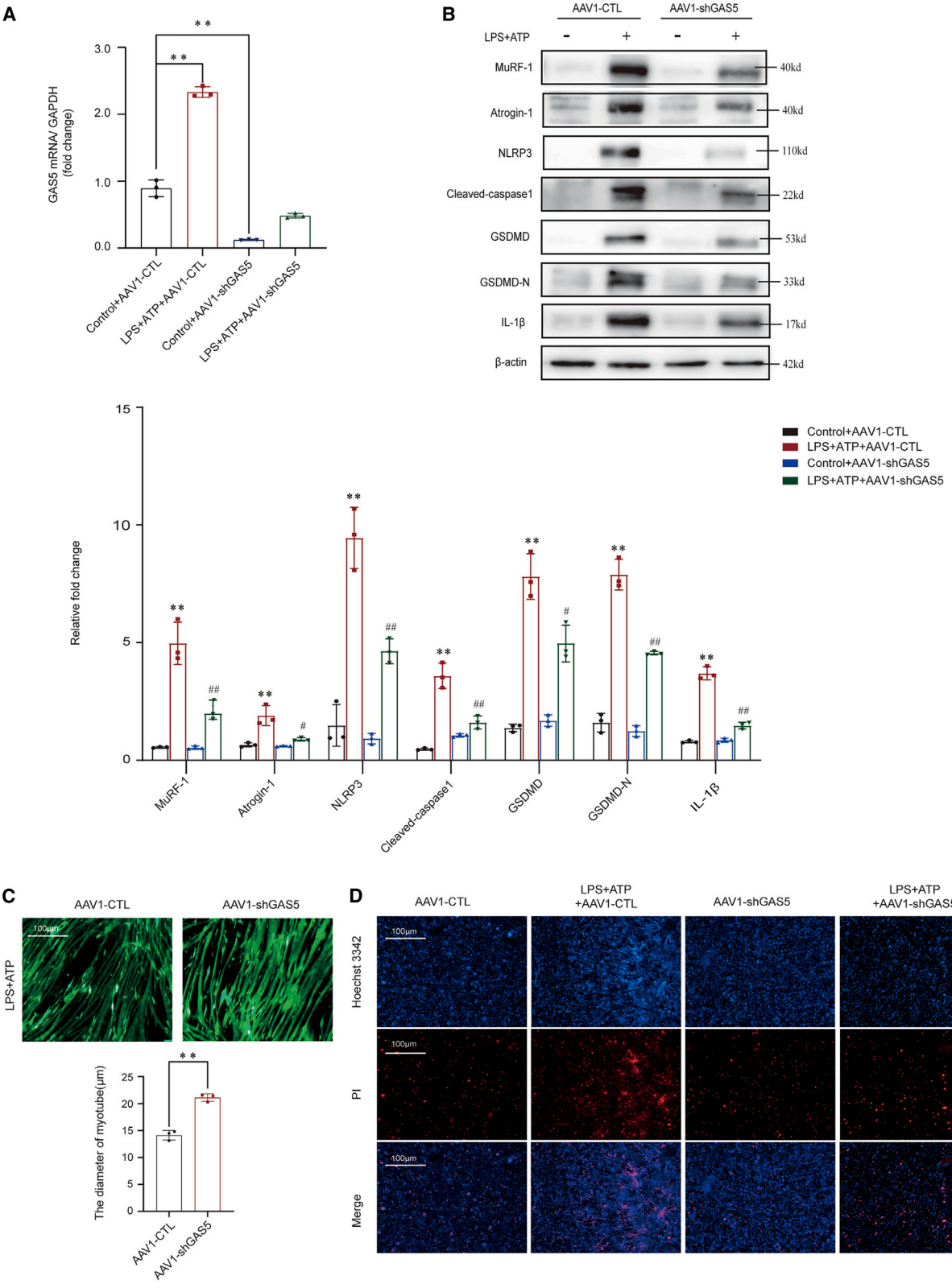


*(legend on next page)*

atrophy caused by CKD, pyroptosis and the NLRP3 signaling pathway are activated, with IL-1β secretion playing a role in the onset and progression of skeletal muscle atrophy.

Increasing evidence suggests that lncRNAs regulate NLRP3-mediated pyroptosis through various mechanisms.[31] In addition to directly interacting with specific proteins, lncRNAs can also form sponges by binding with microRNAs (miRNAs), influencing the expression of NLRP3 mRNA. Luo et al. reported that lncRNA NLRP3 acts as a sponge interacting with miR-138-5p, thereby upregulating the expression of NLRP3.[32] Moreover, lncRNAs can regulate the activation of the NLRP3 inflammasome by modulating the NF-κB signaling pathway.[33] Yi and colleagues found that lncRNA Gm4419 upregulates pro-inflammatory cytokines in mesangial cells of diabetic nephropathy through the NF-κB/NLRP3 pathway.[34] Research has shown that lncRNA Neat1 promotes the assembly of the NLRP3 inflammasome, thus activating the inflammatory response.[35] Like the majority of studies, our research indicated that lncRNA has a positive regulatory effect on the NLRP3 pathway. We found that in CKD-induced muscle atrophy, pyroptosis is activated by lncRNA GAS5 through the NLRP3 signaling pathway. We revealed that GAS5 knockdown downregulated the expression of atrophy-related proteins such as MuRF-1 and Atrogin-1. We also identified that pyroptosis-associated proteins, including NLRP3, cleaved caspase-1, GSDMD, GSDMD-N, and the inflammatory cytokine IL-1β, were markedly suppressed upon GAS5 knockdown. lncRNA does not always exert positive regulation on NLRP3; conversely, lncRNAs can also reduce the expression of NLRP3. For example, lncRNA XLOC_000647 can inhibit the development of pancreatic cancer by suppressing the promoter activity of NLRP3, thus negatively regulating the expression of NLRP3.[36]

This study confirmed that lncRNA GAS5 interacts with TUFM and activates the NLRP3 signaling pathway, leading to skeletal muscle atrophy, suggesting a new mechanism of lncRNA regulation of the NLRP3 signaling pathway. Importantly, using the AAV1-shGAS5 muscle injection method, we demonstrated that inhibiting GAS5 can significantly alleviate cell pyroptosis and muscle atrophy in CKD mice, highlighting the significance of GAS5 in the pathogenesis of muscle atrophy.

Although our study mainly investigated the function of GAS5 in the cytoplasm, given the multifunctionality of lncRNA, we cannot exclude the possibility that GAS5 regulates gene expression in the nucleus. The findings of this study have not been validated in human skeletal muscle samples yet. Our future work will validate the regulatory mechanism of GAS5 on pyroptosis and skeletal muscle atrophy in human muscles, which will make our research results more clinically relevant and practically valuable. Additionally, we need to further study the specific mechanism of pyroptosis in regulating CKD-induced skeletal muscle atrophy, especially the interaction mechanism between GAS5 and TUFM. lncRNAs have many unconfirmed essential physiological functions, and our study provides a basis for identifying the role of GAS5 in the pathogenesis of CKD-induced muscle atrophy.

In conclusion, we have demonstrated that GAS5 interacts with TUFM, promoting the activation of pyroptosis, leading to skeletal muscle atrophy. Inhibiting GAS5 in CKD muscles can suppress the activation of pyroptosis and alleviate muscle atrophy. Our research results offer new insights for the prevention and treatment of CKD-induced muscle atrophy.

## MATERIALS AND METHODS

### Animal and CKD model

All experiments were approved by the Ethics Committee of Xinhua Hospital, Shanghai Jiao Tong University School of Medicine. C57BL/6J mice (12 weeks old) were obtained from Shanghai Slac Laboratory Animal, the previously described two-step 5/6 nephrectomy was used to establish CKD mouse models, and the sham control group underwent anesthesia induction without surgical removal of the kidney mass.[37] Four weeks after 5/6 nephrectomy, CKD mice and sham controls received an intermuscular injection of AAV1 into the quadriceps femoris muscles and were pair fed for another 4 weeks. AAV1 carrying sh-GAS5 (AAV1-shGAS5) and shRNA-scramble (AAV1-CTL) were synthesized by Hanbio Biotechnology, China. The preparation and purification processes of AAV1 vectors were as follows: first, the pHBAAV-U6-MCS-CMV-Zs Green vector was designed, restriction enzyme digestion and ligation were used to construct the plasmid vector, then we confirmed the accuracy of sequence. After virus packaging, using lysis buffer solution to lysis cell. Further purification of the virus was performed after initial purification by ultracentrifugation. The concentrations of the stock solutions of AAV1-shGAS5 and AAV1-CTL were $1.58 \times 10^{10}$ and $2.51 \times 10^{10}$ plaque-forming unit (PFU)/mL, respectively, and the injection dose for both groups was 50 μL. Sham control mice ate the same amount of food as the CKD mice during paired feeding, and this sequence was repeated for the duration of the experiment.

### Cell culture and transfection

The C2C12 mouse myoblasts (ATCC; Manassas, VA, USA) were cultured in Dulbecco's modified Eagle's medium containing 10% fetal bovine serum and 1% penicillin/streptomycin. For differentiating myotubes, C2C12 myoblasts were treated with 2% horse serum for

**Figure 4. Knockdown of GAS5 improves LPS/ATP-induced pyroptosis and atrophy in C2C12 myotubes**

(A) Real-time qPCR confirmed the downregulation of GAS5 in C2C12 myotubes transfected with AAV1-shGAS5 ($n = 3$, $^{**}p < 0.01$). (B) The protein levels of MuRF-1, Atrogin-1, NLRP3, cleaved caspase-1, GSDMD, GSDMD-N, and IL-1β were measured by western blot under different treatment conditions ($n = 3$, $^{**}p < 0.01$ vs. control+AAV1-CTL; $^{\#}p < 0.05$ and $^{\#\#}p < 0.01$ vs. LPS+ATP+AAV1-CTL). (C) Fluorescence images display an improvement in the diameter of LPS/ATP-stimulated C2C12 myotubes transfected with AAV1-shGAS5 (top). Scale bar: 100 μm. Graphic presentation of myotube diameter under different treatment conditions (bottom). (D) Detection of pyroptotic activity in C2C12 myotubes under different treatment conditions by dual staining with Hoechst 33342 and PI.

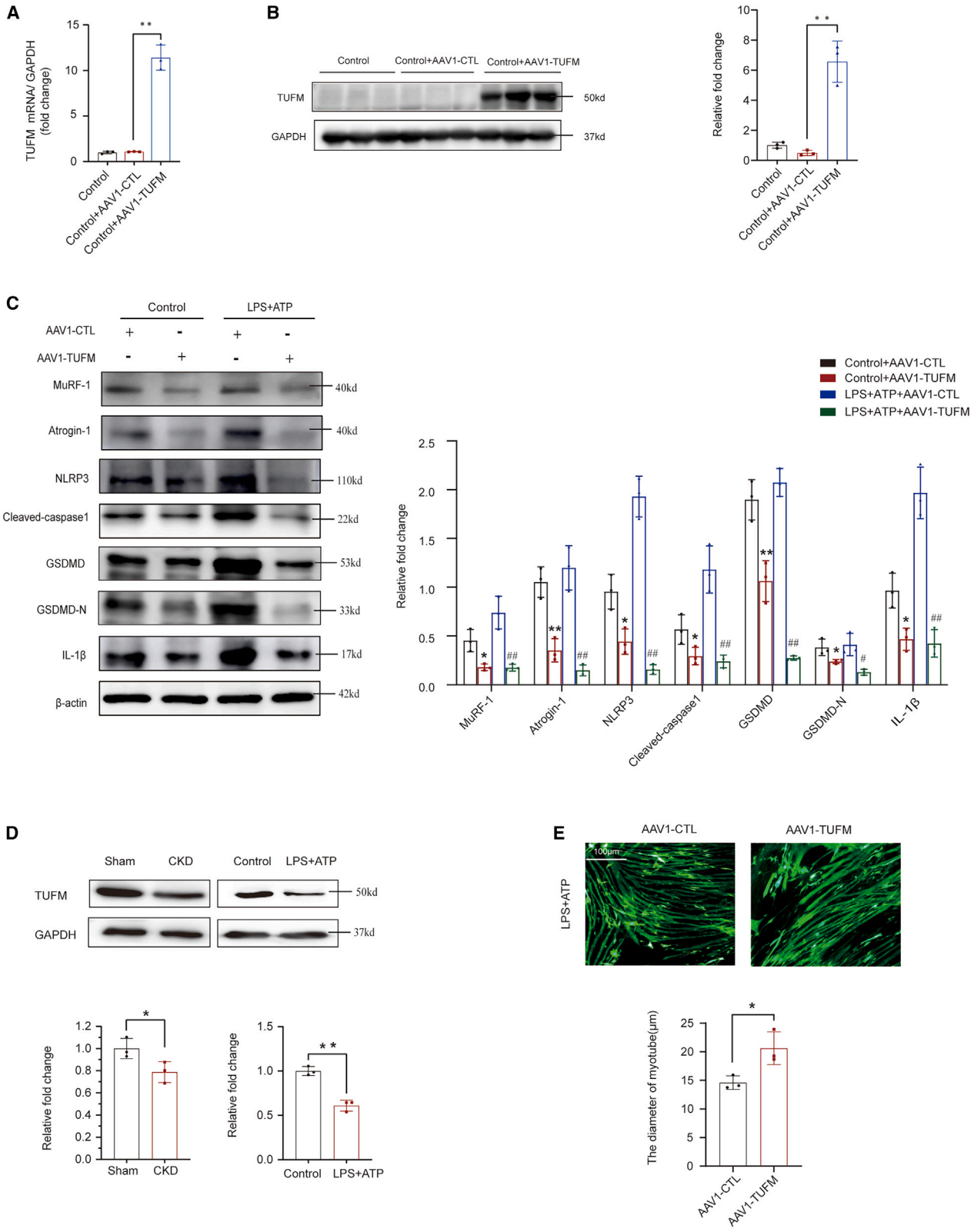


*(legend on next page)*

at least 72 h. In the follow-up experiments, C2C12 myotubes were incubated with LPS (100 ng/mL; Sigma) for 2 h and ATP (5.0 mM; Med Chem Express) for an additional 1 h to cause inflammation.[10] Viral infection was performed at a multiplicity of infection (MOI) of 50 for 24 h. We transfected AAV1-shGAS5 and AAV1-CTL into C2C12 myotubes with concentrations of 2 and 1.25 μL/mL for 48 h. RT-qPCR was performed to measure transfection efficiency. Target sequences of these short hairpin RNAs (shRNA) were as follows: sh-GAS5: 5'-AGAAGATGGTGTCAGATATAT-3' and shRNA-scramble: 5'-TTCT CCG AACGTGTCACGTAA-3'.

#### RNA-seq analysis

The mirVana miRNA Isolation Kit (Ambion, USA) was used to extract the total RNA of quadriceps femoris muscles from mice, in accordance with the manufacturer's protocol. RNA libraries were generated using TruSeq Stranded Total RNA prep kit with Ribo-Zero Gold (Illumina, USA). The DESeq software (R package) was employed to analyze the differentially expressed lncRNAs in CKD mouse models.

#### Histological examination

After being dissected, the gastrocnemius muscles were rinsed with PBS and fixed for 24 h in 4% paraformaldehyde (PFA). Paraffin-embedded muscle tissues were desiccated to make 5-μm slices, H&E staining was performed to examine changes in the CSAs of muscles, and the CSAs was measured by ImageJ.

#### TEM

Gastrocnemius muscles were isolated from mice, cut into pieces no larger than 1 $mm^3$ in volume, and then incubated in electron microscope fixative for 2–4 h at 4°C and rinsed in 0.1 M phosphate buffer (PB; pH 7.4) 3 times. The tissues were fixed in 1% osmium acid-0.1 M PB (pH 7.4) at room temperature (20°C) for 2 h. For dehydration, tissues were sequentially placed in 50% alcohol, 70% alcohol, 80% alcohol, 90% alcohol, 95% alcohol, 100% alcohol, 100% alcohol, 100% acetone, 100% acetone for 15 min each time. The sections were dried with uranium-lead double staining at room temperature overnight after embedding, and a transmission electron microscope was used to analysis the images.

#### IF

The gastrocnemius muscles were isolated, washed with PBS, and fixed in 4% PFA for 24 h. After paraffin-embedded muscle tissues were desiccated, the sections were subjected to an antigen-repair cassette containing EDTA antigen repair buffer (pH 8.0) and placed in a microwave oven. The slides were shaken dry, and an autofluorescence quencher was added, and then they were incubated with anti-mouse NLRP3 (Proteintech, USA, 1:200) and anti-mouse cleaved caspase-1 (Cell Signaling Technology, USA, 1:200) at 4°C overnight after being blocked with 5% goat serum for 30 min. Subsequently, the sections were incubated with secondary antibodies for 1 h at room temperature in the dark. 4-6-diamidino-2-phenylindole was used to stain the nuclei, the changes were examined with a fluorescent microscope (NIKON ECLIPSE C1), and images were captured using the NIKON DS-U3 imaging system.

#### Western blotting and antibodies

The proteins were extracted from C2C12 myotubes and quadriceps muscles of mice. The concentrations of immunoreactive proteins were measured using ImageJ and normalized to the concentrations of β-actin or GAPDH. The primary antibodies used were as follows: anti-MuRF-1 (Santa Cruz, USA, sc-398608), anti-Atrogin-1 (ECM Biosciences, USA, AP2041), anti-NLRP3 (Cell Signaling Technology, USA, 15101S), anti-GSDMD (Abcam, USA, ab209845), anti-GSDMD-N (Abcam, USA, ab209845), anti-cleaved caspase-1 (Cell Signaling Technology, USA, 89332S), anti-IL-1β (Abcam, USA, ab2105), anti-GAPDH (Proteintech, USA, ag16692), and anti-β-actin (Servicebio, China, GYW00011).

#### FISH

The FISH assay was conducted in C2C12 myotubes and gastrocnemius muscles of mice. The sections were digested with proteinase K (20 μg/mL) for 5 min after being fixed in 4% PFA for 20 min, rinsed with PBS, and incubated at 37°C for 1 h; we dropwise added the prehybridization solution and hybridization solution (containing a probe GAS5 concentration of 1 μM) and hybridized the sections at 42°C overnight. After washing off the hybridization solution, we performed DAPI staining for 8 min. Subsequently, an anti-fluorescence quenching sealer was added to seal the sections. A Nikon orthomosaic fluorescence microscope was used to observe the images. The probe information of GAS5: 5′-CCATCACAGAGGTCCACACTGCCAT TCCTGCT-3' FAM labeling.

#### RNA pull-down assay and MS

PCR amplification was performed to screen for suitable PCR primers for the sense and antisense strands, and the PCR products were used as templates and then transcribed *in vitro* to obtain pure lncRNA GAS5 using the MAXIscript kit (Thermo Fisher Scientific). The transcribed lncRNA GAS5 was mixed with biotinylated cytidine bisphosphate and incubated at −20°C overnight to obtain biotin-labeled lncRNA GAS5. The labeled lncRNA GAS5 was incubated with streptavidin magnetic beads for 30 min at room temperature and

**Figure 5. TUFM overexpression counteracts GAS5-driven NLRP3 activation and pyroptosis in C2C12 myotubes**

(A) Real-time qPCR result shows increased TUFM mRNA levels after the overexpression of TUFM in C2C12 myotubes ($n = 3$, $^{**}p < 0.01$). (B) Western blot confirmed the protein level of TUFM was increased after the overexpression of TUFM in C2C12 myotubes ($n = 3$, $^{**}p < 0.01$). (C) The protein levels of MuRF-1, Atrogin-1 NLRP3, cleaved caspase-1, GSDMD, GSDMD-N, and IL-1β were measured by western blot under different treatment conditions ($n = 3$, $^{*}p < 0.05$ and $^{**}p < 0.01$ vs. control+AAV1-CTL; $\#p < 0.05$ and $\#\#p < 0.01$ vs. LPS+ATP+AAV1-CTL). (D) The downregulation of TUFM was confirmed by immunoblots in CKD mice (left) and LPS/ATP-treated C2C12 myotubes (right) ($n = 3$, $^{*}p < 0.05$ and $^{**}p < 0.01$). (E) Fluorescence images display an improvement in the diameter of LPS/ATP-stimulated C2C12 myotubes by TUFM overexpression (top). Scale bar: 100 μm. Graphic presentation of myotube diameter in different groups (bottom).

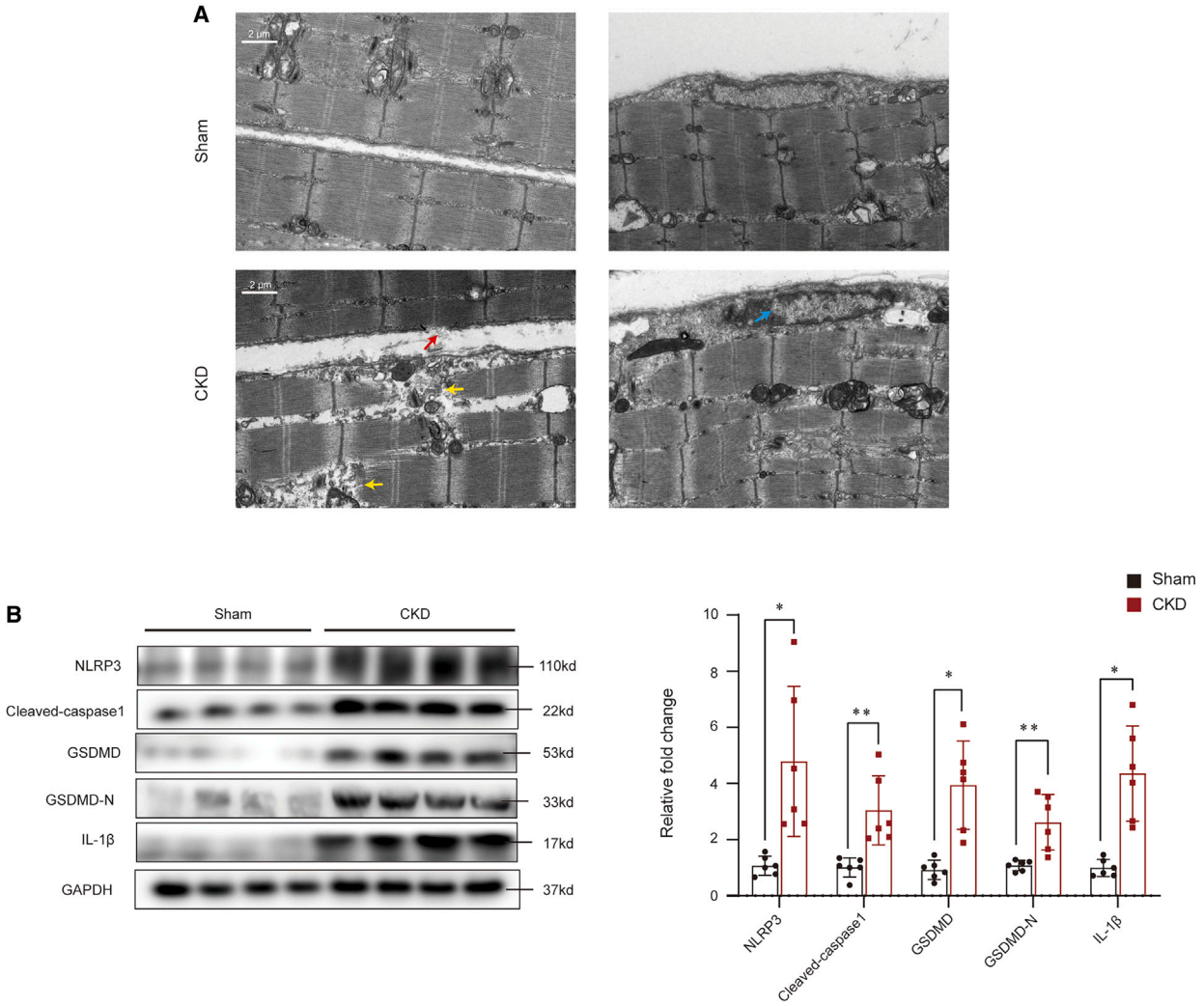


*(legend on next page)*

incubated with pre-prepared C2C12 cytoplasmic lysates and nucleus lysates at 4°C for 1 h. Following incubation, the beads were collected and washed once by adding 200 μL 1× washing buffer. 200 μL 1× washing buffer was added and mixed with the beads again. We put the mixture into a magnetic stand, discarded the supernatant, and then added 100 μL elution buffer and vortexed to mix it well, followed by incubation for 15 min at room temperature. Subsequently, we added 20 μL of elution buffer and boiled it for 5 min, placed the centrifuge tube on a magnetic stand for 2 min, and removed the supernatant. Silver staining was used to detect proteins that were separated by sodium dodecyl sulfate-polyacrylamide gel electrophoresis (SDS-PAGE). The primer sequences were as follows: lncRNA GAS5 sense F2, 5'-TAATACGACTCACTATAGGGGTCTTTTCGAGGTAGGAGTCGACTCCTGTG-3'; lncRNA GAS5 sense R2, 5'-TTTTTTTTTTTTTTTTTTTTTTTGATGGGATTGCA-3'; lncRNA GAS5 antisense F2, 5'-TAATACGACTCACTATAGGGTTTTTTTTTTTTTTTTTTGATGGATTGCA-3'; and lncRNA GAS5 antisense R2, 5'-GTCTTTTCGAGGTAGGAGTCGACTCCTGTG-3'. The RNA-binding protein complexes were washed, eluted, and analyzed by MS. The MS was performed by LC-BIO Biotech (Hangzhou, China).

### RIP

RIP experiments were conducted using RIP kit (BersinBio, China, Bes5101), complying with the manufacturer's instructions. RNA was co-immunoprecipitated using anti-TUFM antibody (1:20, ABclonal, USA, A6423). Anti-TUFM (Proteintech, USA, 67802-1-Ig) was used for western blotting, and RT-PCR was performed to measure the expression of GAS5.

### Statistical analysis

SPSS 25.0 was used for the statistical analysis, and all data are presented as mean ± SD. To evaluate the differences in the two groups, we used two-tail unpaired Student's t tests, while two-way ANOVA was performed for more than two groups. $^{*}p < 0.05$ and $^{**}p < 0.01$ were considered statistically significant.

## DATA AND CODE AVAILABILITY

The data generated in this study are available upon request from the corresponding author.

## ACKNOWLEDGMENTS

This study is not supported by relevant fundings. This study has been authorized by the ethics committee of Xinhua Hospital, which is a part of Shanghai Jiaotong University's School of Medicine.

## AUTHOR CONTRIBUTIONS

L.S. was responsible for the whole study and the submission of the final version. R.H. was responsible for conducting the experiment, analyzing the data, interpreting the findings, and writing the article. S.L. and X.T. assisted in the completion of the experiment.

## DECLARATION OF INTERESTS

The authors declare no potential conflicts of interest with respect to the research, authorship, and/or publication of this article.

## SUPPLEMENTAL INFORMATION

Supplemental information can be found online at https://doi.org/10.1016/j.omtn.2025.102451.

## REFERENCES

1. Francis, A., Harhay, M.N., Ong, A.C.M., Tummalapalli, S.L., Ortiz, A., Fogo, A.B., Fliser, D., Roy-Chaudhury, P., Fontana, M., Nangaku, M., et al. (2024). Chronic kidney disease and the global public health agenda: an international consensus. Nat. Rev. Nephrol. *20*, 473–485.
2. Schardong, J., Marcolino, M.A.Z., and Plentz, R.D.M. (2018). Muscle Atrophy in Chronic Kidney Disease. Adv. Exp. Med. Biol. *1088*, 393–412.
3. Tsuji, J., Thomson, T., Chan, E., Brown, C.K., Oppenheimer, J., Bigelow, C., Dong, X., Theurkauf, W.E., Weng, Z., and Schwartz, L.M. (2020). High-resolution analysis of differential gene expression during skeletal muscle atrophy and programmed cell death. Physiol. Genom. *52*, 492–511.
4. Morgan, J.E., Prola, A., Mariot, V., Pini, V., Meng, J., Hourde, C., Dumonceaux, J., Conti, F., Relaix, F., Authier, F.J., et al. (2018). Necroptosis mediates myofibre death in dystrophin-deficient mice. Nat. Commun. *9*, 3655.
5. Kroemer, G., Galluzzi, L., Vandenabeele, P., Abrams, J., Alnemri, E.S., Baehrecke, E.H., Blagosklonny, M.V., El-Deiry, W.S., Golstein, P., Green, D.R., et al. (2009). Classification of cell death: recommendations of the Nomenclature Committee on Cell Death 2009. Cell Death Differ. *16*, 3–11.
6. Xue, Y., Enosi Tuipulotu, D., Tan, W.H., Kay, C., and Man, S.M. (2019). Emerging Activators and Regulators of Inflammasomes and Pyroptosis. Trends Immunol. *40*, 1035–1052.
7. Shi, J., Zhao, Y., Wang, K., Shi, X., Wang, Y., Huang, H., Zhuang, Y., Cai, T., Wang, F., and Shao, F. (2015). Cleavage of GSDMD by inflammatory caspases determines pyroptotic cell death. Nature *526*, 660–665.
8. Kayagaki, N., Stowe, I.B., Lee, B.L., O'Rourke, K., Anderson, K., Warming, S., Cuellar, T., Haley, B., Roose-Girma, M., Phung, Q.T., et al. (2015). Caspase-11 cleaves gasdermin D for non-canonical inflammasome signalling. Nature *526*, 666–671.
9. He, W.T., Wan, H., Hu, L., Chen, P., Wang, X., Huang, Z., Yang, Z.H., Zhong, C.Q., and Han, J. (2015). Gasdermin D is an executor of pyroptosis and required for interleukin-1beta secretion. Cell Res. *25*, 1285–1298.
10. Wang, L., Jiao, X.F., Wu, C., Li, X.Q., Sun, H.X., Shen, X.Y., Zhang, K.Z., Zhao, C., Liu, L., Wang, M., et al. (2021). Trimetazidine attenuates dexamethasone-induced muscle atrophy via inhibiting NLRP3/GSDMD pathway-mediated pyroptosis. Cell Death Dis. *7*, 251.
11. Liu, Y., Bi, X., Zhang, Y., Wang, Y., and Ding, W. (2020). Mitochondrial dysfunction/NLRP3 inflammasome axis contributes to angiotensin II-induced skeletal muscle wasting via PPAR-gamma. Lab. Invest. *100*, 712–726.
12. Aluganti Narasimhulu, C., and Singla, D.K. (2021). Amelioration of diabetes-induced inflammation mediated pyroptosis, sarcopenia, and adverse muscle remodelling by bone morphogenetic protein-7. J. Cachexia Sarcopenia Muscle *12*, 403–420.
13. Xu, X.D., Li, K.R., Li, X.M., Yao, J., Qin, J., and Yan, B. (2014). Long non-coding RNAs: new players in ocular neovascularization. Mol. Biol. Rep. *41*, 4493–4505.
14. Chen, L.L., and Zhao, J.C. (2014). Functional analysis of long noncoding RNAs in development and disease. Adv. Exp. Med. Biol. *825*, 129–158.
15. Wang, Y.W., Dong, H.Z., Tan, Y.X., Bao, X., Su, Y.M., Li, X., Jiang, F., Liang, J., Huang, Z.C., Ren, Y.L., et al. (2022). HIF-1α-regulated lncRNA-TUG1 promotes

**Figure 6. Evidence linking pyroptosis to muscle atrophy in CKD mice**

(A) TEM confirmed the morphological characteristics of pyroptosis in muscles of CKD mice. Large sections of cell membrane (CM) displaying discontinuities, forming extensive holes (red arrows), with partial rupture of muscle fibers (yellow arrows, left). Irregularly shaped nuclei (N) and chromatin condensation were found in the CKD group (blue arrows, right). (B) The protein levels of NLRP3, cleaved caspase-1, GSDMD, GSDMD-N, and IL-1β in quadriceps muscles of mice were measured by western blot ($n = 7$, $^{*}p < 0.05$ and $^{**}p < 0.01$). (C) Immunofluorescence staining underscored heightened expression of NLRP3 (red) and cleaved caspase-1 (green) in CKD mice muscles.

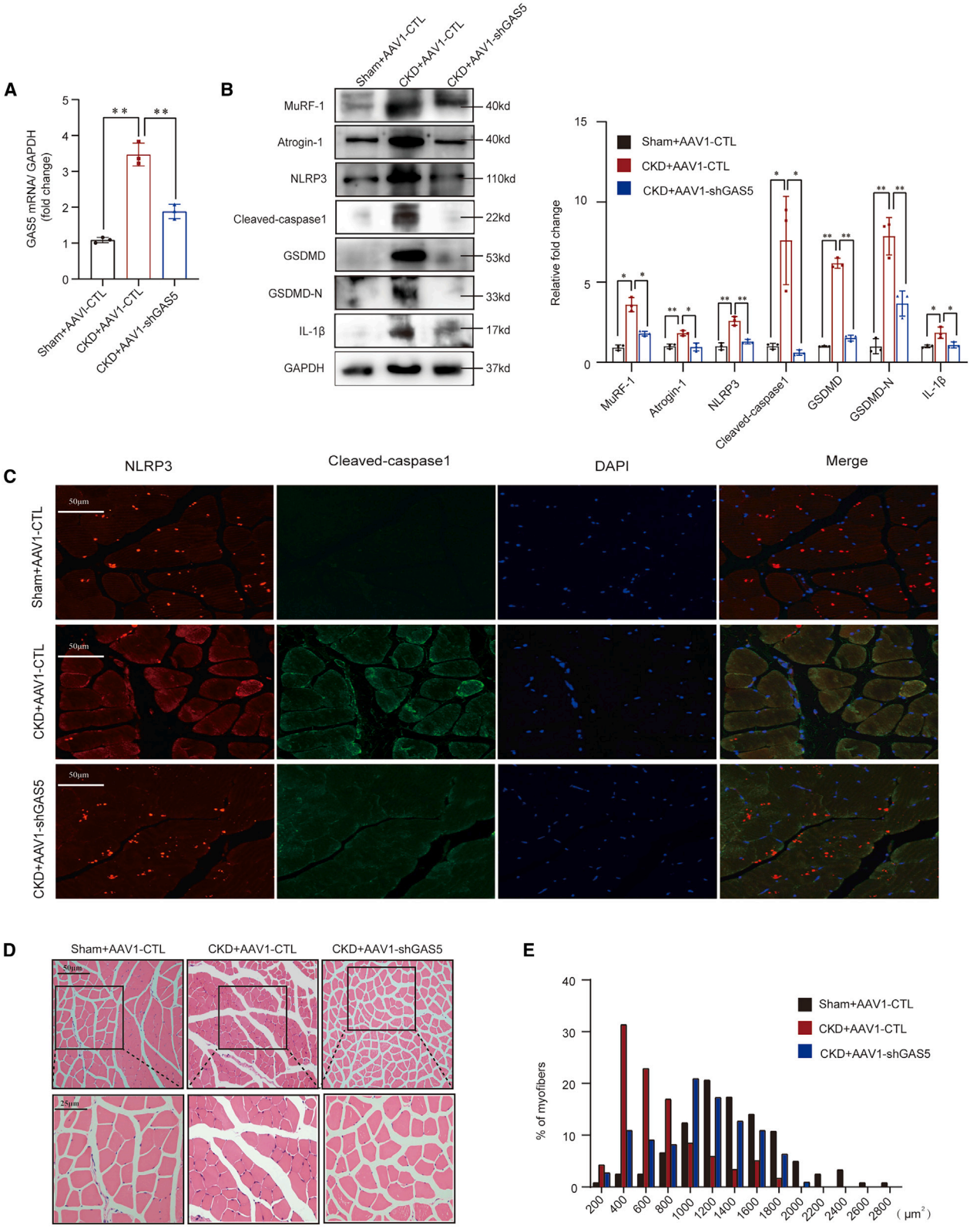


*(legend on next page)*

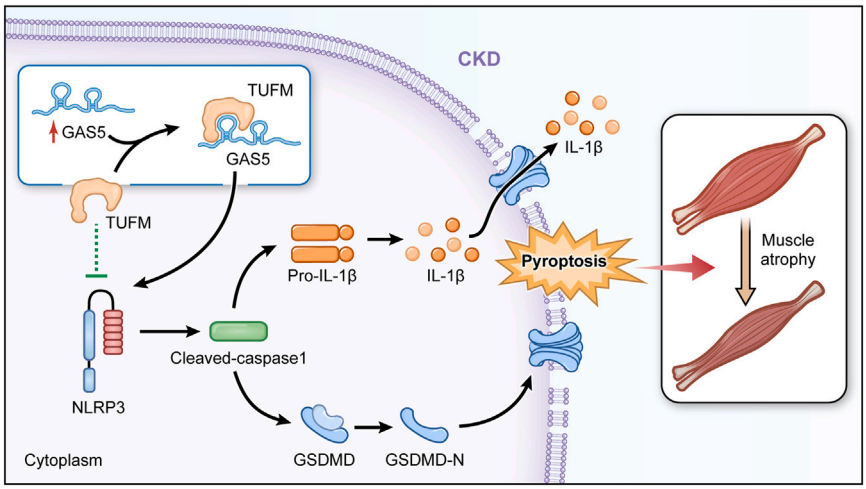


**Figure 8. A summative diagram of GAS5 regulates pyroptosis in skeletal muscle atrophy with CKD**

GAS5 interacts with TUFM, and this interaction promotes NLRP3 activation, consequently activating the pyroptosis pathway and leading to the occurrence of pyroptosis and muscle atrophy in CKD.

mitochondrial dysfunction and pyroptosis by directly binding to FUS in myocardial infarction. Cell Death Dis. *8*, 178.

16. Li, J., Lin, J., Ji, Y., Wang, X., Fu, D., Wang, W., and Shen, B. (2023). A novel pyroptosis-associated lncRNA LINC01133 promotes pancreatic adenocarcinoma development via miR-30b-5p/SIRT1 axis. Cell. Oncol. *46*, 1381–1398.

17. Song, H., Yang, B., Li, Y., Qian, A., Kang, Y., and Shan, X. (2022). Focus on the Mechanisms and Functions of Pyroptosis, Inflammasomes, and Inflammatory Caspases in Infectious Diseases. Oxid. Med. Cell. Longev. *2022*, 2501279.

18. Gao, L., Jiang, Z., Han, Y., Li, Y., and Yang, X. (2022). Regulation of Pyroptosis by ncRNA: A novel research direction. Front. Cell Dev. Biol. *10*, 840576.

19. Meng, L., Lin, H., Huang, X., Weng, J., Peng, F., and Wu, S. (2022). METTL14 suppresses pyroptosis and diabetic cardiomyopathy by downregulating TINCR lncRNA. Cell Death Dis. *13*, 38.

20. Sun, L., Si, M., Liu, X., Choi, J.M., Wang, Y., Thomas, S.S., Peng, H., and Hu, Z. (2018). Long-noncoding RNA Atrolnc-1 promotes muscle wasting in mice with chronic kidney disease. J. Cachexia Sarcopenia Muscle *9*, 962–974.

21. Li, M., Gou, H., Tripathi, B.K., Huang, J., Jiang, S., Dubois, W., Waybright, T., Lei, M., Shi, J., Zhou, M., and Huang, J. (2015). An Apela RNA-Containing Negative Feedback Loop Regulates p53-Mediated Apoptosis in Embryonic Stem Cells. Cell Stem Cell *16*, 669–683.

22. Chu, C., Zhang, Q.C., da Rocha, S.T., Flynn, R.A., Bharadwaj, M., Calabrese, J.M., Magnuson, T., Heard, E., and Chang, H.Y. (2015). Systematic discovery of Xist RNA binding proteins. Cell *161*, 404–416.

23. Tian, C., Min, X., Zhao, Y., Wang, Y., Wu, X., Liu, S., Dou, W., Zhou, T., Liu, Y., Luo, R., et al. (2022). MRG15 aggravates non-alcoholic steatohepatitis progression by regulating the mitochondrial proteolytic degradation of TUFM. J. Hepatol. *77*, 1491–1503.

24. Ding, J., Li, F., Cong, Y., Miao, J., Wu, D., Liu, B., and Wang, L. (2019). Trichostatin A inhibits skeletal muscle atrophy induced by cigarette smoke exposure in mice. Life Sci. *235*, 116800.

25. Liu, Y., Wang, D., Li, T., Yang, F., Li, Z., Bai, X., and Wang, Y. (2022). The role of NLRP3 inflammasome in inflammation-related skeletal muscle atrophy. Front. Immunol. *13*, 1035709.

26. Yan, B., Zhang, Y., Liang, C., Liu, B., Ding, F., Wang, Y., Zhu, B., Zhao, R., Yu, X.Y., and Li, Y. (2020). Stem cell-derived exosomes prevent pyroptosis and repair ischemic muscle injury through a novel exosome/circHIPK3/FOXO3a pathway. Theranostics *10*, 6728–6742.

27. Park, E., Choi, H., Truong, C.S., and Jun, H.S. (2023). The Inhibition of Autophagy and Pyroptosis by an Ethanol Extract of Nelumbo nucifera Leaf Contributes to the Amelioration of Dexamethasone-Induced Muscle Atrophy. Nutrients *15*, 804.

28. Liu, D., Xiao, Y., Zhou, B., Gao, S., Li, L., Zhao, L., Chen, W., Dai, B., Li, Q., Duan, H., et al. (2021). PKM2-dependent glycolysis promotes skeletal muscle cell pyroptosis by activating the NLRP3 inflammasome in dermatomyositis/polymyositis. Rheumatology *60*, 2177–2189.

29. Huang, N., Kny, M., Riediger, F., Busch, K., Schmidt, S., Luft, F.C., Slevogt, H., and Fielitz, J. (2017). Deletion of Nlrp3 protects from inflammation-induced skeletal muscle atrophy. Intensive Care Med. Exp. *5*, 3.

30. Al-Kuraishy, H.M., Al-Gareeb, A.I., and Al-Nami, M.S. (2019). Vinpocetine Improves Oxidative Stress and Pro-Inflammatory Mediators in Acute Kidney Injury. Int. J. Prev. Med. *10*, 142.

31. Luo, D., Liu, F., Zhang, J., Shao, Q., Tao, W., Xiao, R., Dai, W., and Qian, K. (2021). Functional crosstalk between Long non-coding RNAs and the NLRP3 inflammasome in the regulation of diseases. Mol. Immunol. *131*, 191–200.

32. Luo, D., Dai, W., Feng, X., Ding, C., Shao, Q., Xiao, R., Zhao, N., Peng, W., Yang, Y., Cui, Y., et al. (2021). Suppression of lncRNA NLRP3 inhibits NLRP3-triggered inflammatory responses in early acute lung injury. Cell Death Dis. *12*, 898.

33. Samra, Y.A., Said, H.S., Elsherbiny, N.M., Liou, G.I., El-Shishtawy, M.M., and Eissa, L.A. (2016). Cepharanthine and Piperine ameliorate diabetic nephropathy in rats: role of NF-kappaB and NLRP3 inflammasome. Life Sci. *157*, 187–199.

34. Yi, H., Peng, R., Zhang, L.Y., Sun, Y., Peng, H.M., Liu, H.D., Yu, L.J., Li, A.L., Zhang, Y.J., Jiang, W.H., and Zhang, Z. (2017). LincRNA-Gm4419 knockdown ameliorates

**Figure 7. Knockdown of GAS5 alleviates cellular pyroptosis and muscle atrophy in CKD mice**

(A) Real-time qPCR confirmed the expression of GAS5 mRNA in quadriceps muscles transfected with AAV1-shGAS5 or AAV1-CTL ($n = 3$, $^{**}p < 0.01$). (B) Protein levels of MuRF-1, Atrogin-1, NLRP3, cleaved caspase-1, GSDMD, GSDMD-N, and IL-1β in quadriceps muscles of mice were determined by western blot ($n = 3$, $^{*}p < 0.05$ and $^{**}p < 0.01$). (C) Immunofluorescence staining determined the expression of NLRP3 (red) and cleaved caspase-1 (green) in quadriceps muscles transfected with AAV1-shGAS5 or AAV1-CTL. (D) H&E staining shows the CSAs of mice muscles transfected with AAV1-shGAS5 or AAV1-CTL (scale bars: top, 50 μm and bottom, 25 μm; magnified images). (E) The distribution of myofiber sizes in CKD mice transfected with AAV1-shGAS5 was shifted rightward compared with CKD mice transfected with AAV1-CTL.

NF-kappaB/NLRP3 inflammasome-mediated inflammation in diabetic nephropathy. Cell Death Dis. *8*, e2583.

35. Zhang, P., Cao, L., Zhou, R., Yang, X., and Wu, M. (2019). The lncRNA Neat1 promotes activation of inflammasomes in macrophages. Nat. Commun. *10*, 1495.

36. Hu, H., Wang, Y., Ding, X., He, Y., Lu, Z., Wu, P., Tian, L., Yuan, H., Liu, D., Shi, G., et al. (2018). Long non-coding RNA XLOC_000647 suppresses progression of pancreatic cancer and decreases epithelial-mesenchymal transition-induced cell invasion by down-regulating NLRP3. Mol. Cancer *17*, 18.

37. Souza, A.C.P., Tsuji, T., Baranova, I.N., Bocharov, A.V., Wilkins, K.J., Street, J.M., Alvarez-Prats, A., Hu, X., Eggerman, T., Yuen, P.S.T., and Star, R.A. (2015). TLR4 mutant mice are protected from renal fibrosis and chronic kidney disease progression. Phys. Rep. *3*, e12558.